ANL/EBR-037

OPERATION OF EBR-II AS AN IRRADIATION FACILITY AT 62.5 MWt: AN EVALUATION OF PLANT AND REACTOR DATA FROM RUN 46A

Coordinated by

R. A. Cushman

Major Contributors

H. W. Buschman
R. A. Cushman
I. A. Engen
H. A. Larson
R. W. Hyndman
J. R. Karvinen
F. S. Kirn
J. K. Long
L. B. Miller
C. L. Nelson
W. H. Perry
C. C. Price
R. R. Smith
V. N. Thompson
M. R. Tuck
W. R. Wallin

EBR-II Project
Argonne National Laboratory
Argonne, Illinois - Idaho Falls, Idaho

February 1971

Work performed under the auspices of the U. S. Atomic Energy Commission

DISCLAIMER

TABLE OF CONTENTS

LIST OF FIGURES

LIST OF TABLES

OPERATION OF EBR-II AS AN IRRADIATION FACILITY AT 62.5 MWt: AN EVALUATION OF PLANT AND REACTOR DATA FROM RUN 46A

Coordinated by

R. A. Cushman

ABSTRACT

The initial operation of EBR-II at 62.5 MWt occurred during run 38A in September 1969, with a core containing no fueled experimental subassemblies. Run 38A indicated that the reactor and plant were capable of sustained operation at 62.5 MWt. After interim operation at 50 MWt, during which minor adjustments were made to the plant and experimenters were informed of the plan to operate continually at 62.5 MWt, run 46A was scheduled as the first to contain fueled experimental subassemblies and operate routinely at the higher power level. Experimental subassemblies were modified and relocated as required to match the higher-power conditions, and run 46A was begun. The reactor and plant were monitored during the run, and several special tests were carried out. As a result of the tests, the recommendation is made to continue operation of EBR-II at 62.5 MWt.

I. INTRODUCTION

Since 1968 a continuous effort has been made to increase the operating power level of EBR-II to its design power of 62.5 MWt while the reactor fulfills its current primary role in the AEC's LMFBR program as an irradiation facility and engineering test bed. In August, 1968, the reactor power was increased from the previous maximum operating level of 45 MWt to 50 MWt; in September,1969, according to plan,[1] a special core loading was installed in EBR-II and the power level was increased, during run 38A only, to 62.5 MWt.[2] That operation indicated that the EBR-II reactor and power plant

could perform at 62.5 MWt. A reduction in power to 50 MWt was necessary while experimenters were informed of plans to proceed to routine operation at 62.5 MWt and existing experimental subassemblies were redesigned for those reactor conditions. Plans were then made for continual operation at 62.5 MWt,[3] and such operation began on September 25, 1970. This report presents results of special tests and observations made during run 46A, the first of the routine runs at the design power of EBR-II.

II. CORE LOADING

The increase in power from 50 to 62.5 MWt required that several experimental subassemblies, which were designed for operation in specific locations in the reactor at 50 MWt, be repositioned for 62.5-MWt operation. Some subassemblies required only relocating to a new core position farther from the reactor center. Other subassemblies, however, had to be removed from the reactor and disassembled, with the experimental elements being reconstituted in new subassemblies. Reconstitution of experimental subassemblies was required because the subassembly lower adapter is different for rows 1 through 5 than for rows 6 and 7, as is the outer blanket adapter. The reconstitution posed no problem in accommodating the experiments in the reactor at higher power. There was, however, a scheduling difficulty, in that all of the experimental subassemblies being irradiated at 50 MWt could not be reconstituted during the shutdown between runs 45 and 46. Some of them were, therefore, removed and modified during run 45, while others were modified during run 46 and thus were not in the reactor during the initial increase in power with fueled experiments.

Therefore, the core loading for run 46, although it contained experimental subassemblies (in contrast to the initial 62.5-MWt operation during run 38A), was not a typical EBR-II loading. It contained 20 experimental subassemblies. Run 44B, in contrast, contained 32 experimental subassemblies, and run 47B is expected to contain 29. The actual core loading for run 46A is shown in Fig. 1. It was an 88-subassembly core, with depleted-uranium blanket subassemblies in three row-6 positions for reactivity control. There were fueled experimental subassemblies in row 7, and two of them (X058 and X062) contained sufficient fuel that depleted-uranium blanket

KEY:

B - DEPLETED URANIUM
BETH - BERYLLIUM THIMBLE
C# - CONTROL ROD
CF - CONTROLLED-FLOW SUBASSEMBLY
D - DRIVER FUEL
EBU - EXTENDED-BURNUP SUBASSEMBLY
MK-II - MARK-II FUEL
Ni - NICKEL-CORROSION SUBASSEMBLY
P - ½DRIVER FUEL -- ½ STAINLESS STEEL
R - STAINLESS STEEL REFLECTOR
S# - SAFETY ROD
SSCR - STAINLESS STEEL CONTROL ROD
SSTH - STAINLESS STEEL THIMBLE
70% - 70% - ENRICHED DRIVER FUEL
- EXPERIMENTAL SUBASSEMBLY

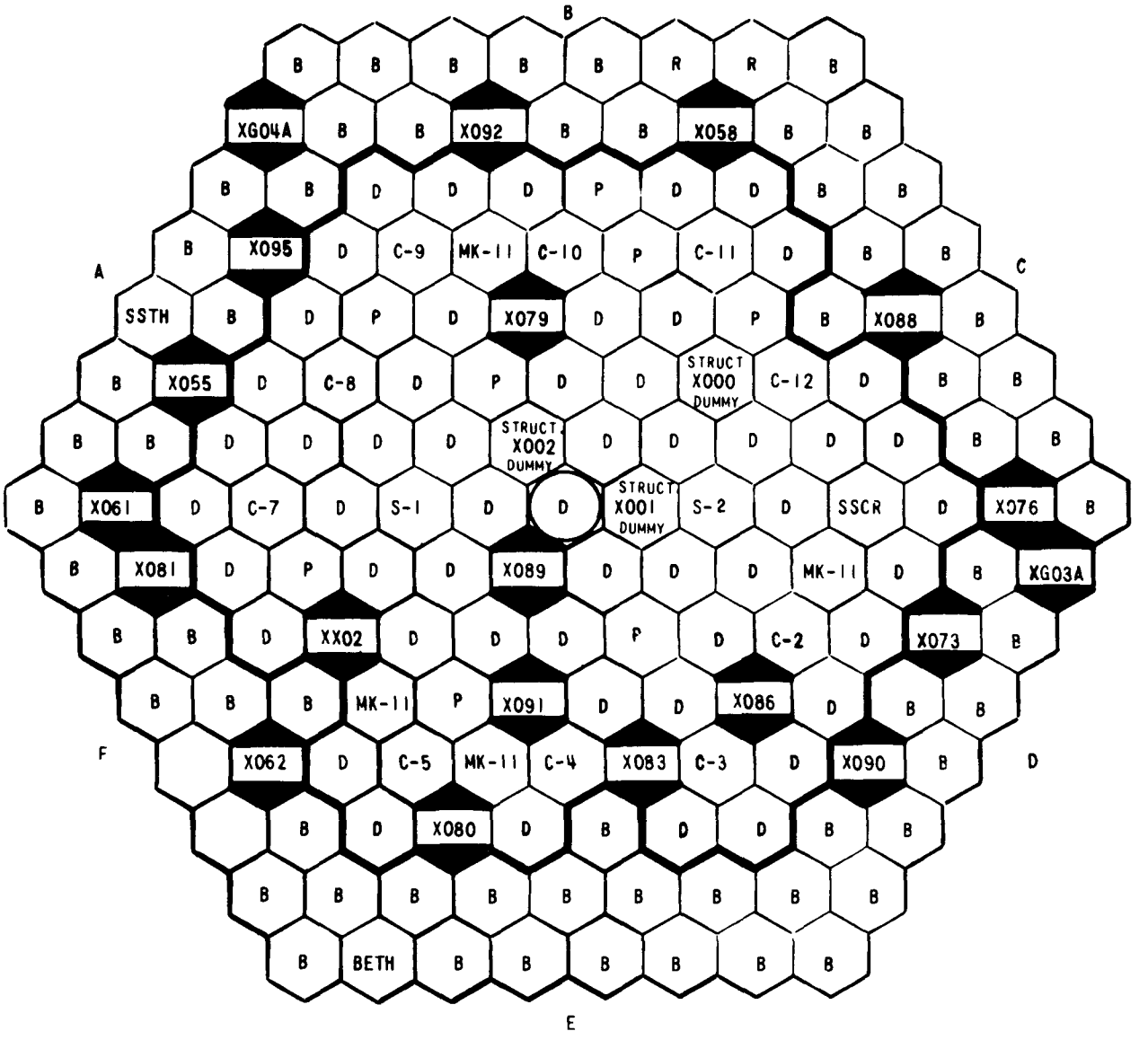

Fig. 1. Loading Pattern for EBR-II Run 46A

subassemblies next to them in row 8 would have overheated. Two stainless steel reflector subassemblies, identical in appearance to the blanket subassemblies but containing solid stainless steel rods rather than uranium clad with stainless steel, were used in place of two depleted-uranium blanket subassemblies immediately outboard of each of the heavily fueled experimental subassemblies. Table I lists the experimental subassemblies that were loaded for run 46A, with pertinent information concerning them. Three dummy structural experimental subassemblies and nine half-worth subassemblies (containing 46 fuel elements and 45 stainless steel rods rather than 91 fuel elements) were loaded in the core for reactivity control and to simulate, in terms of loading, future experimental subassemblies. The stainless steel drop rod used in feedback analysis was in control-rod position 1.

III. PROCEDURE AND EXPERIMENTAL PLAN

The generally successful completion of run 38A in September,1969, indicated that continual operation of the EBR-II reactor and plant at 62.5 MWt could commence as soon as the experimental subassemblies could be modified as required. There were, however, slight difficulties with some components (e.g., bypass steam valve) during run 38A, which were to be corrected during the interval. In addition, the run-46A core loading included fueled experiments, unlike that for run 38A. A test procedure was, therefore, prepared for run 46A: "Reactor and Plant Systems Performance Test and Surveillance for Power Increase from 50 MWt to 62.5 MWt and Continued Operation at 62.5 MWt."

The major specific areas covered by the test procedure, other than surveillance of plant conditions that changed owing to the higher-power operation, were:

1. A set of flux-wire irradiations at 50 kWt to determine whether the fission-rate distribution for the revised core loading (experimental subassemblies moved generally farther from the core center) was similar to that for previous cores, as calculations had indicated;

2. Rod-drop measurements at zero power (500 kWt) and at 50, 56, and 62.5 MWt for reactivity determinations;

TABLE I. Experimental Subassemblies in EBR-II during Run 46A

Subassembly Number and (Position)	Date Charged	Capsule Content and (Number of Capsules)		Experimenter	Reconstituted
XX02 (5F3)	4/13/70	UO_2-25 wt % PuO_2	(36)	HEDL	No
XG03A (8D2)	9/14/70	UO_2-20 wt % PuO_2	(2)	GE	Yes
XG04A (8A7)	9/15/70	UO_2-20 wt % PuO_2	(2)	GE	No
X055 (7A3)	2/23/69	$(U_{0.85}$-$Pu_{0.15})C$	(19)	UNC	No
X058 (7B6)	4/24/69	UO_2-25 wt % PuO_2	(37)	GE	No
X061 (7A1)	4/23/69	Structural	(7)	INC	No
X062 (7F3)	5/23/69	UO_2-25 wt % PuO_2	(37)	GE	No
X073 (7D3)	12/12/69	UO_2-25 wt % PuO_2	(37)	HEDL	No
X076 (7D1)	3/27/70	UO_2-25 wt % PuO_2	(19)	WARD	No
X079 (4B2)	4/17/70	$(U_{0.85}$-$Pu_{0.15})C$	(19)	UNC	No
X080 (6E5)	9/11/70	UO_2-20 wt % PuO_2 Structural Structural	(12) (1) (4)	NUMEC/ANL GE GE	No
X081 (7F6)	5/24/70	UO_2-25 wt % PuO_2	(9)	GE	No
X083 (5E2)	9/15/70	Mark-IA fuel	(61)	ANL	No
X086 (5E2)	8/7/70	$(U_{0.8}$-$Pu_{0.2})N$ $(U_{0.8}$-$Pu_{0.2})C$ $(U_{0.8}$-$Pu_{0.2})C$	(10) (5) (4)	BMI LASL WARD	No
X088 (7C4)	5/24/70	UO_2-25 wt % PuO_2	(19)	WARD	No

Table I (contd)

Subassembly Number and (Position)	Date Charged	Capsule Content and (Number of Capsules)		Experimenter	Reconstituted
X089 (2F1)	9/15/70	Structural	(7)	HEDL	No
X090 (7D5)	9/15/70	Structural	(4)	BMI	No
		Structural	(1)	INC	
		Structural	(1)	ORNL	
		Structural	(1)	HEDL	
X091 (4E3)	9/11/70	Structural	(7)	HEDL	No
X092 (7B3)	9/15/70	Structural	(1)	LASL	No
X095 (7A5)	9/18/70	Structural	(1)	NRL	No

3. Determinations of power-reactivity decrements up to 62.5 MWt with the new core loading;

4. Acoustic-noise recordings of the sodium-to-superheated-steam heat exchanger, to determine the effect, if any, of a higher rate of flow of secondary sodium at higher power, and similar recordings of the primary pumps to obtain an operating signature of these pumps; and

5. Determination of the effects of improvements in the plant system made since run 38A. Three specific changes were made:

a. Large Steam Bypass Valve (P3-VC-501A)

The pneumatic controls for the valve were replaced with electronic components. This change has greatly reduced the lag time of the system. A new "V-pup" plug was installed in the valve.

b. Turbine-driven Feedwater Pump

The turbine-driven feedwater pump was overhauled after run 38A. In addition, the discharge check valve of the motor-driven pump was not tightly closed during run 38A. A damaged seat ring prevented the disk from seating, and thus allowed backflow through the turbine-driven pump so that its capacity was decreased. The check valve has been repaired, and a stepwise improvement was noted in the performance of the turbine-driven pump at 50 MWt.

c. 13.8 kV - 480 V Transformers

Cooling fans have been installed on the two 13.8 kV - 480 V transformers. This installation has increased the capacity of each transformer from 2000 to 2300 kVA, so that either transformer can handle the entire load if the other should fail.

IV. REACTOR OPERATION

A. Fission Rates

Run 46A began, as planned, with irradiation at 50 kWt of uranium-wire detectors. Extensive calculations had been made before run 46 to give confidence that the experimental subassemblies could be relocated without compromising the relative heat ratings. However, because of the many changes, this

confidence was verified with measured fission rates. Consequently, three special wire subassemblies were loaded into the reactor in positions 1A1, 5A2, and 6D3. Two ^{235}U-wire detectors were placed in each subassembly, and one ^{238}U-wire detector was placed in position 1A1 and two in 6D3. These samples, all at the axial midplane, were irradiated for 1 hr at an estimated 50 kW. The measured relative fission rates in ^{235}U are compared with calculated values in Table II. The calculated values were obtained from both DOT X-Y problems and from the BURNUP code for the run-46A loading.

It was concluded from these data that, within the core region of the reactor, the relative flux distribution would be adequately described by the distribution used for the runs before the loading changes, until the extensive fission-rate map is determined during run 49 or 50.

In addition to the relative fission rates, absolute fission rates were obtained for the central subassembly. Table III lists the results from this measurement. From Table III, a calibration of power can be made by using the same relative fission rate-distribution normally used in the BURNUP code.

Estimates from the above data indicate the test was run at an equivalent of 46.7 kW. From the thermal calibration at 50 MWt and the ratio of the channel-7 data of Table III, the power level was estimated at 49.2 kW. This ratio of 0.95 for the two estimates further confirms previous findings that the ratio of burnup rates measured from fission-product determination to those of the EBR-II BURNUP code is 0.95.

Curves showing the relative radial fission rate for several cores, including the measured values obtained with the run-29D loading, were given in Fig. 2 of Ref. 3. This figure is reproduced here as Fig. 2, but superimposed on the figure is the local/average fission-density distribution for the run-46A core loading. The distribution is, as can be seen from Fig. 2, similar to all of the projected 62.5-MWt cores with experimental subassemblies, as well as that measured for run 29D. The curve for run 46A, as for the other calculated curves, was obtained by taking the average fission rate for all driver-fuel subassemblies in a given type of core position (e.g., 3N2, 5N2) as calculated by the POWER subroutine of the DOT X-Y problem for the given core loading.

TABLE II. Comparison of Measured and Calculated Fission Rates for Run 46A

Subassembly Position	Foil Number	Radius,[a] cm	^{235}U Fission Rate (Relative) Measured	DOT-5	BURNUP	Ratios DOT-5 / Measured	Ratios BURNUP / Measured
1A1	2	2.6	1.00		1.00		
	3	2.6	0.982		1.00		
			avg 0.99	1.00	1.00	1.01	1.01
5A2	2	19.1	0.846		0.834		0.99
	4	23.4	0.758		0.743		0.98
			avg 0.802	0.818	0.789	1.02	0.98
6D3	4	23.8	0.741		0.705		0.95
	2	27.7	0.649		0.607		0.94
			avg 0.695	0.647	0.656	0.93	0.94

[a]Geometric center.

TABLE III. Absolute Fission Rate and Power-calibration Data

Total fission ^{235}U, fissions/g ^{235}U	0.292×10^{13}
Total fission ^{238}U, fissions/g ^{238}U	0.187×10^{12}
Length of run, sec	3650
Channel-7 reading,A	$48.1\% \times 10^{-7}$
Channel-7 reading @ 50 MWt, A	$48.9\% \times 10^{-4}$
BURNUP code normalization, fissions/g - MWd @ 200 MeV/fission (central fission rate)	1.51×10^{16}

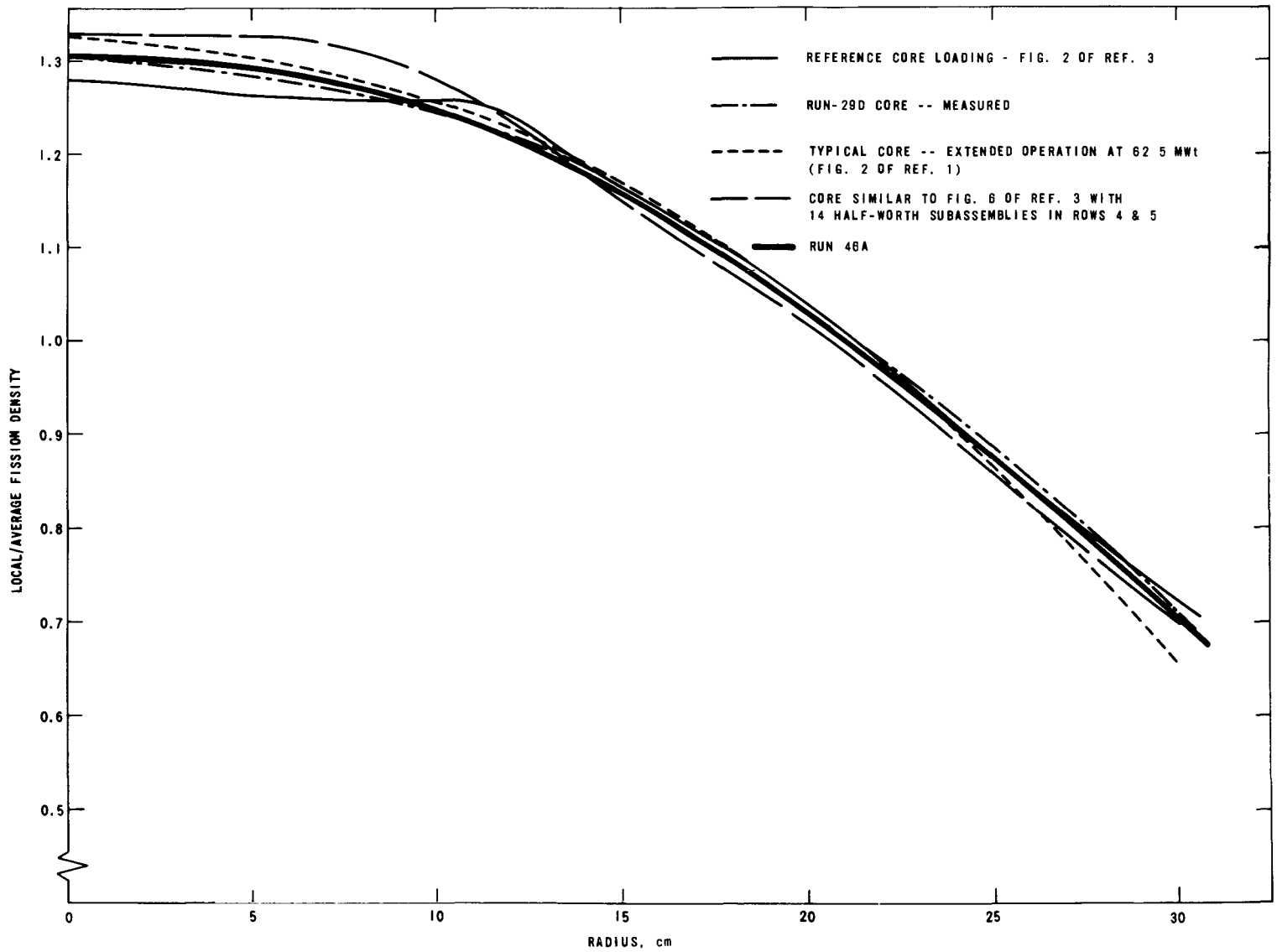

Fig. 2. Radial Distribution of Relative Fission Rates in Driver-fuel Subassembly

B. Power Distribution

Because the radial fission-rate distribution for the run-46A core was so similar to that for similar projected 62.5-MWt core loadings with experimental subassemblies, the actual power distribution among subassemblies was also similar to projected cases. This similarity is shown in Table IV, which reproduces Table I from Ref. 3, with the addition of a column of subassembly powers for run 46A. The power per driver-fuel subassembly for the actual loading, with the exception of rows 1 and 2 (which are off by less than 1%), lies between values projected for the cores presented in the proposals for 62.5-MWt operation (Refs. 1 and 3). Each value in Table IV is the power produced in a standard EBR-II Mark-IA driver-fuel subassembly if it were placed in the particular location in the given core. (There may not always be a standard driver-fuel subassembly in a given position; e.g., 5N1 and 5N3 normally contain control-rod subassemblies, and any location could contain an experimental subassembly.) Also shown in Table IV is the number of effective driver-fuel subassemblies that constitute the given core. An effective driver-fuel subassembly is one that corresponds in power density to a standard one. A safety rod, for instance, is 61/91 of an effective driver-fuel subassembly.

The first column in Table IV (after that for core position) is for the actual run-46A core. The second is for the reference loading for 62.5-MWt operation with experimental subassemblies, from Ref. 3. The third column is for the extended-operation core, from Ref. 1. The last two columns present data relevant to the all-driver-fuel core originally analyzed for 62.5-MWt operation. The fourth column gives data from ANL-5719 (Addendum). The last column gives corresponding results for the all-driver-fuel core with the same core loading and fission distribution as in ANL-5719 (Addendum), with temperatures calculated by current methods utilizing the POWDIST program. The last two columns show the significant effect of core size on power distribution and peak power density by comparison with the first two columns. The increase in the number of effective subassemblies in a 91-subassembly core over that analyzed in ANL-5719 (Addendum) assures that the power density must decrease to less than that of the original configuration. Small changes in further irradiation loadings at 62.5 MWt will not significantly affect the subassembly temperature distributions.

TABLE IV. Power Distribution (in kW) per Standard Driver-fuel Subassembly for Various Cores at 62.5 MWt

Core Position	Actual Run-46A Core	Projected 62.5-MWt Cores		ANL-5719 (Addendum) Core	
		Fig. 1 of Ref. 3	Fig. 2 of Ref. 1	Book Value[a]	Recently Calculated[b]
1N1	995	983	986	1177	1147
2N1	978	972	967	1146	1114
3N1	926	948	917	1090	1014
3N2	944	963	933	----	1047
4N1	830	845	825	----	865
4N2, 3	869	887	864	965	922
5N1	701	712	688	----	689
5N2, 4	755	767	747	785	761
5N3	774	786	767	----	786
6N1	552	569	520	----	----
6N2, 5	616	624	585	----	----
6N3, 4	650	658	627	615	621
Number of Effective Driver-fuel Sub-assemblies in Configuration	72.3	72.4	74.1	62.3	62.3

[a]Cited in ANL-5719 (Addendum)

[b]Recalculation of ANL-5719 (Addendum) configuration using current thermal-hydraulic methods.

C. Other Data and Analyses for Run 46A

Information concerning the power-reactivity decrement (PRD), rod-drop studies, feedback-model studies, the use of the Sigma-5 on-line computer to process rod-drop data, the on-line reactivity meter, subassembly-outlet temperatures, the instrument probe, and noise-signature analysis was obtained for run 46A. This information is given below.

1. Power-reactivity Decrement (PRD)

Power-coefficient measurements were made at approximate 10-MWt increments during the ascent to 62.5 MWt at the start of run 46A and during the shutdown at the end of run 46A. Figure 3 compares the data from these measurements with data taken during runs 45A and 38A. (For Run 38A, see Introduction.)

The slight upward bend between 50 and 62.5 MWt in the PRD curve for run 38A is also apparent in the curve for run 46A. This effect is believed to have originated from an increase in the fraction of fuel material entering the gamma phase at the higher temperatures associated with 62.5-MWt operation.

2. Rod-drop Studies

The reactor was started up and brought to a power level of 50 MWt on September 21. After a series of rod drops at 50 MWt, the power level was reduced to 500 kWt to calibrate the reactivity worth of the drop rod. Additional rod drops were made and the power level again was increased to 50 MWt. Rod drops were repeated at 50 MWt, and the resulting feedback data were used to predict the feedback at 56 MWt. Then the power level was increased to 56 MWt, additional rod drops were made, and the resulting feedback data were used to predict the feedback at 62.5 MWt. The power level was increased to the goal of 62.5 MWt on September 25, and rod-drop measurements were repeated at this power level.

Typical rod-drop data are shown in Figs. 4 and 5, which give the power and computed feedback recovery at 50 and 62.5 MWt, respectively.

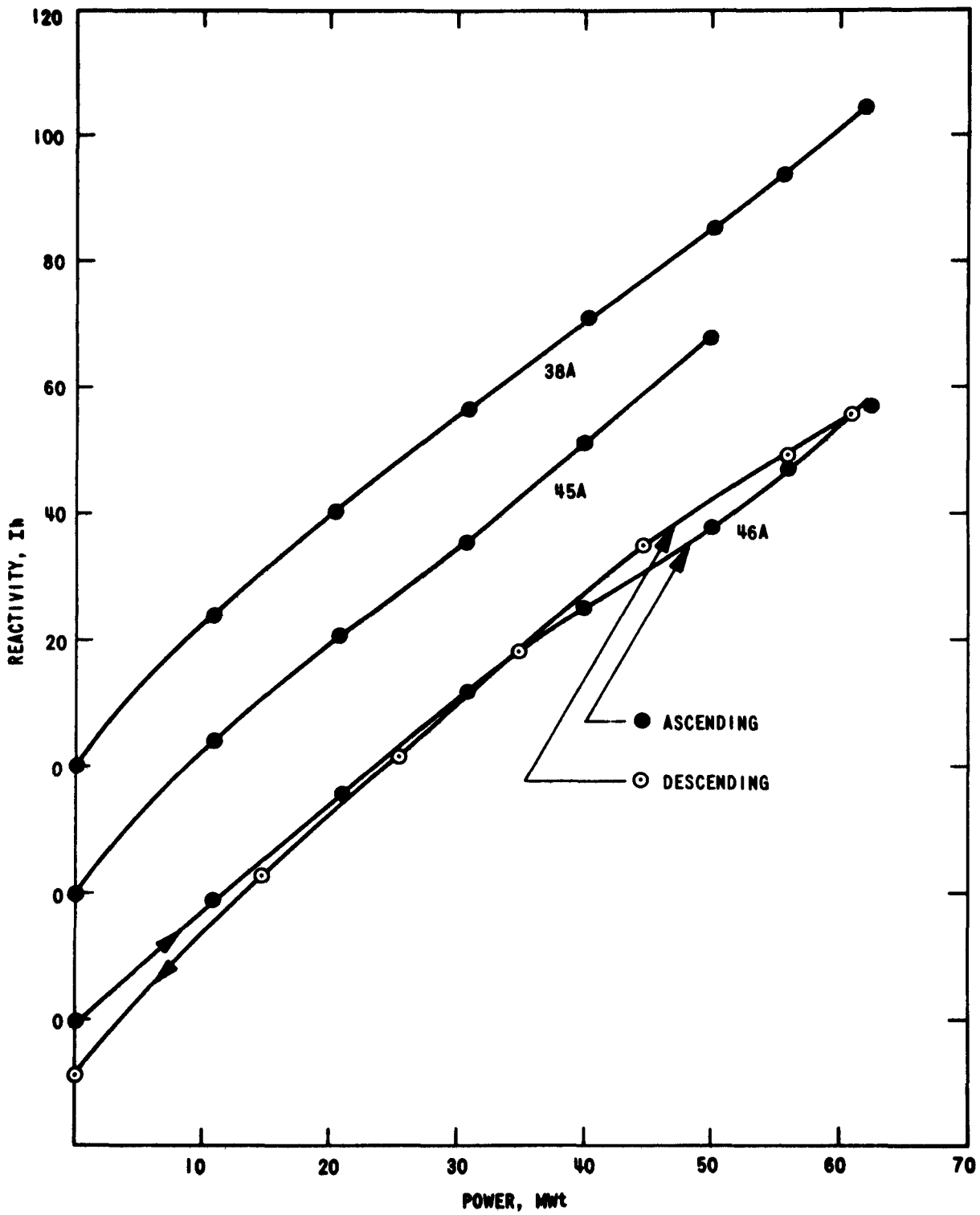

Fig. 3. Power-reactivity Decrement (PRD) for Runs 38A, 45A, and 46A (curves offset for separate viewing)

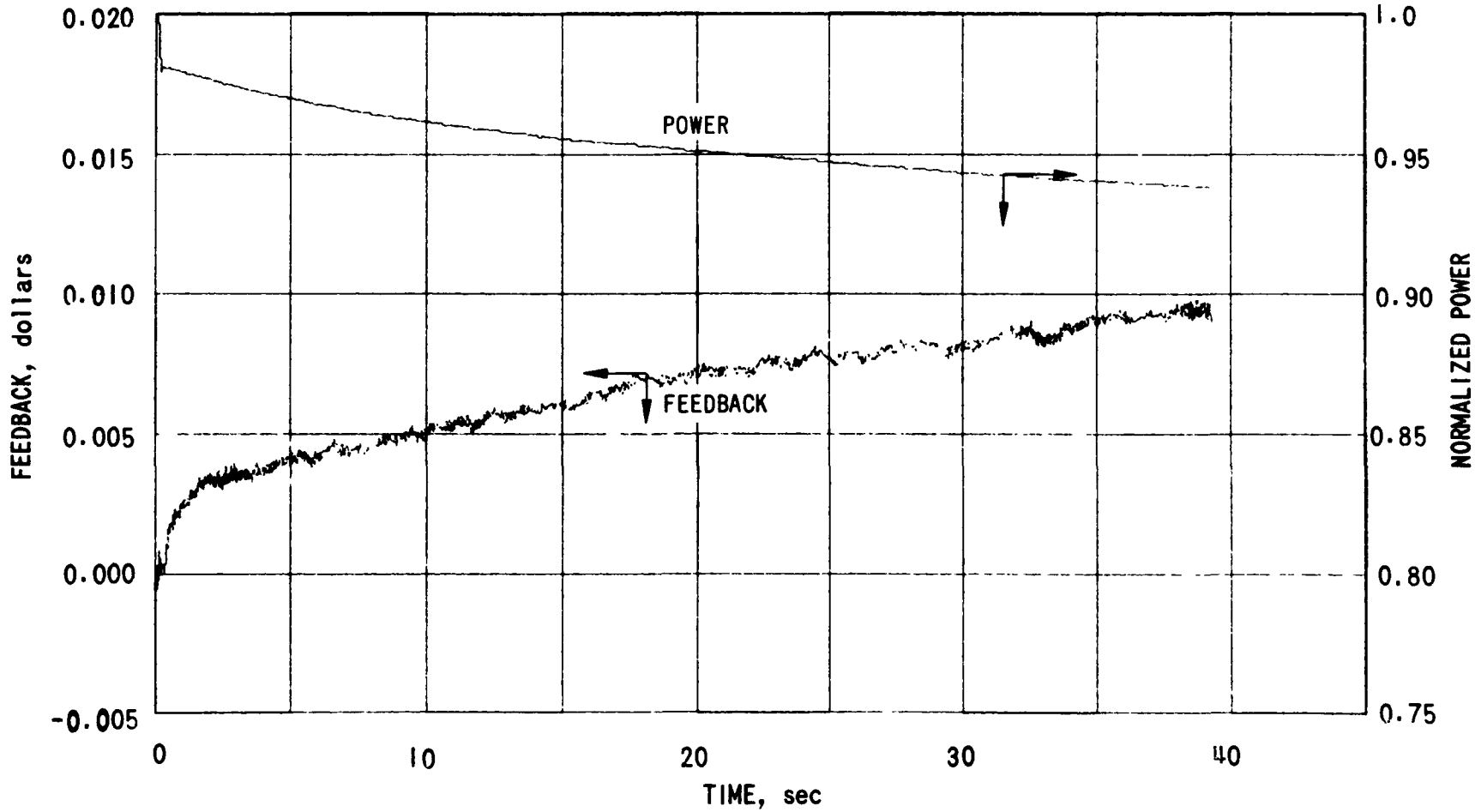

Fig. 4. Power and Negative Feedback at 50 MWt at Start of Run 46A (average from five rod drops)

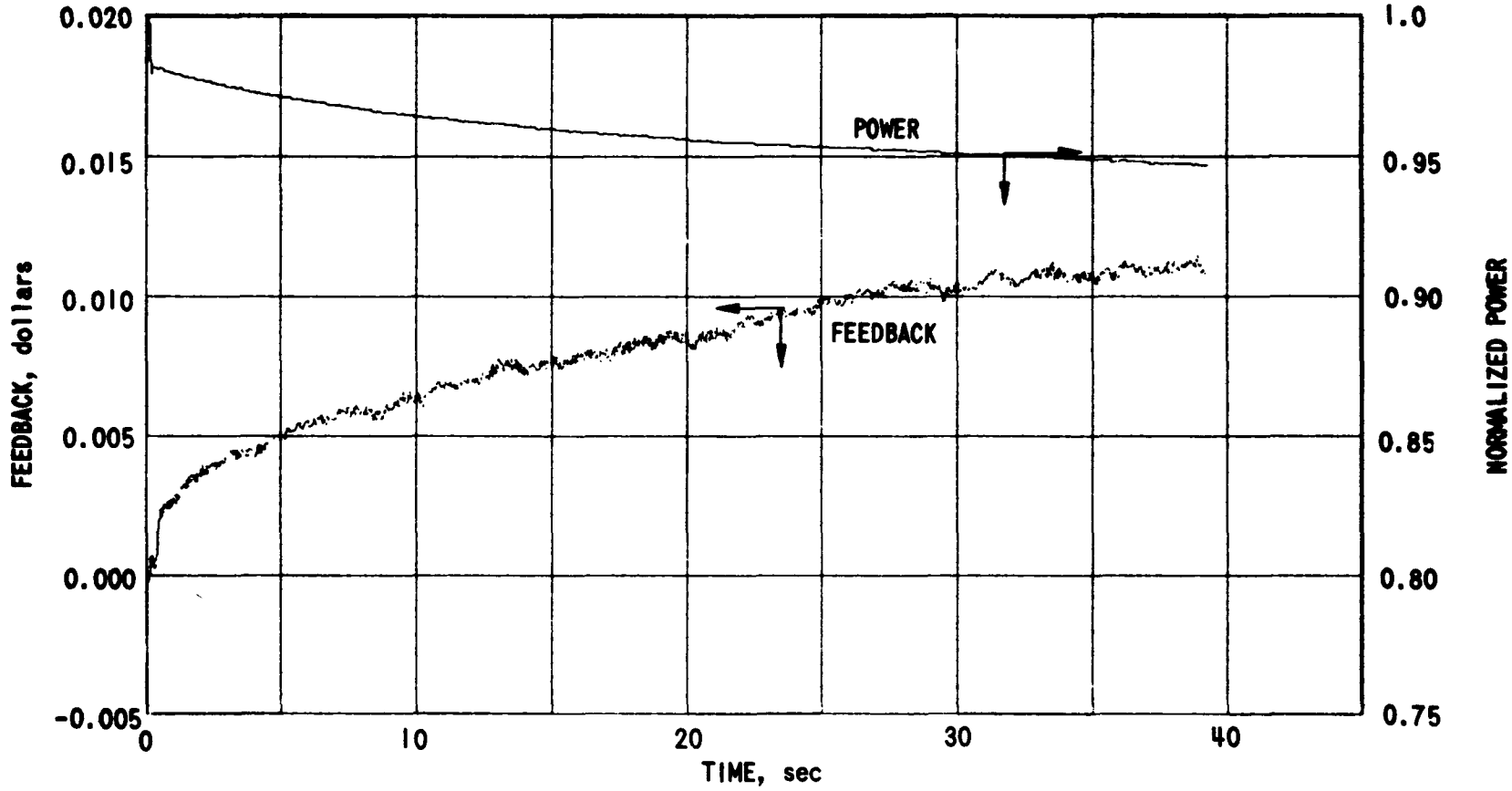

Fig. 5. Power and Negative Feedback at 62.5 MWt at Start of Run 46A (average from four rod drops)

At both powers, the feedback is negative and is prompt in the time interval 0-2 sec after the drop. Similar data sets (not illustrated) were taken over the power range from 62.5 to 40.0 MWt at the end of run 46A. Reference 4 contains a detailed analysis of the rod-drop experiments.

3. Feedback-model Studies

As cited in the preceding section, the feedback measured at 50 MWt was used to predict the feedback at 56 MWt. Similarly, the feedback measured at 56 MWt was used to predict that at 62.5 MWt. The method involved the fitting of feedback data to a mathematical model in the manner described by Hyndman and Nicholson.[5] Then, the coefficients (amplitudes) of each feedback term in the model were increased by the ratio of the power increase, and the feedback-recovery function was recomputed. Power was increased to the next level, and the measured feedback was compared with the predicted feedback.

The models, which incorporate the best-fit values for amplitudes and time constants, were as follows:

Power Level, MWt	Feedback Model
50	$-H(S) = \frac{0.1}{1 + 0.2S} + \frac{0.048}{1 + 0.4S} - \frac{0.018}{1 + 2.0S}$
56	$-H(S) = \frac{0.085}{1 + 0.2S} + \frac{0.0312}{1 + 0.4S} + \frac{0.037}{1 + 2.0S} + \frac{0.0341e^{-5.0S}}{1 + 5.4S}$
62.5	$-H(S) = \frac{0.095}{1 + 0.2S} + \frac{0.0335}{1 + 0.4S} + \frac{0.051}{1 + 2.0S} + \frac{0.020e^{-5.0S}}{1 + 5.4S}$

The amplitudes in these models are expressed in units of dollars of reactivity and are defined as the product of the power level (in megawatts) and the differential power coefficient of reactivity (in dollars of reactivity per megawatt). The feedback, -H, is a complex number and is expressed in dollars of reactivity. S is the complex operator, $i\omega$, where ω is oscillation frequency in radians/sec. Hence, when S = 0 (i.e., when the reactor is operating under steady-state conditions), -H defines the PRD

(power-reactivity decrement), which is the amount of reactivity required to bring the system from hot critical to the power level at which the measurements were made.

In the models, a positive amplitude defines a negative feedback effect. Similarly, a negative amplitude indicates a positive feedback effect.

If feedback effects in the range of 50-62.5 MWt were truly linear, a simple multiplication of the amplitude for the 50-MWt model by the factor 62.5/50 should give the amplitudes measured at 62.5 MWt. An inspection of the values in the models, however, shows that the feedback over the range of 50-62.5 MWt is not strictly linear. On the other hand, multiplication of the amplitudes for the 56-MWt model by the factor 62.5/56 does give reasonable predictions of the 62.5-MWt feedback function. Figure 6 compares the measured data with those calculated from the model given in the figure.

4. Processing Rod-drop Data with the Sigma-5 On-line Computer

Two methods were used for processing rod-drop data during run 46A. One was the conventional method, which uses the IBM-1620 and IBM-360/75 computers. The other method used the recently installed Sigma-5 data-processing system, otherwise known as the digital data-acquisition system (DAS),[6] supplied by Xerox Data Systems.

Figure 7 compares rod-drop feedback data processed by the two methods. The continuous curve for feedback was derived from an analysis made in the conventional manner. The open circles are values derived from the Sigma-5 analysis. The agreement is excellent, as it was with all other rod-drop data processed by the two methods during run 46A. This excellent agreement indicates that the Sigma-5 system is operational for on-line processing of rod-drop data. (The data presented in Figs. 4 and 5 were processed with the Sigma-5 system.)

5. On-line Reactivity Meter

Figure 8 shows reactivity-meter recordings for rod drops at 50, 56, and 62.5 MWt. Apparent is the negative-feedback recovery in the first

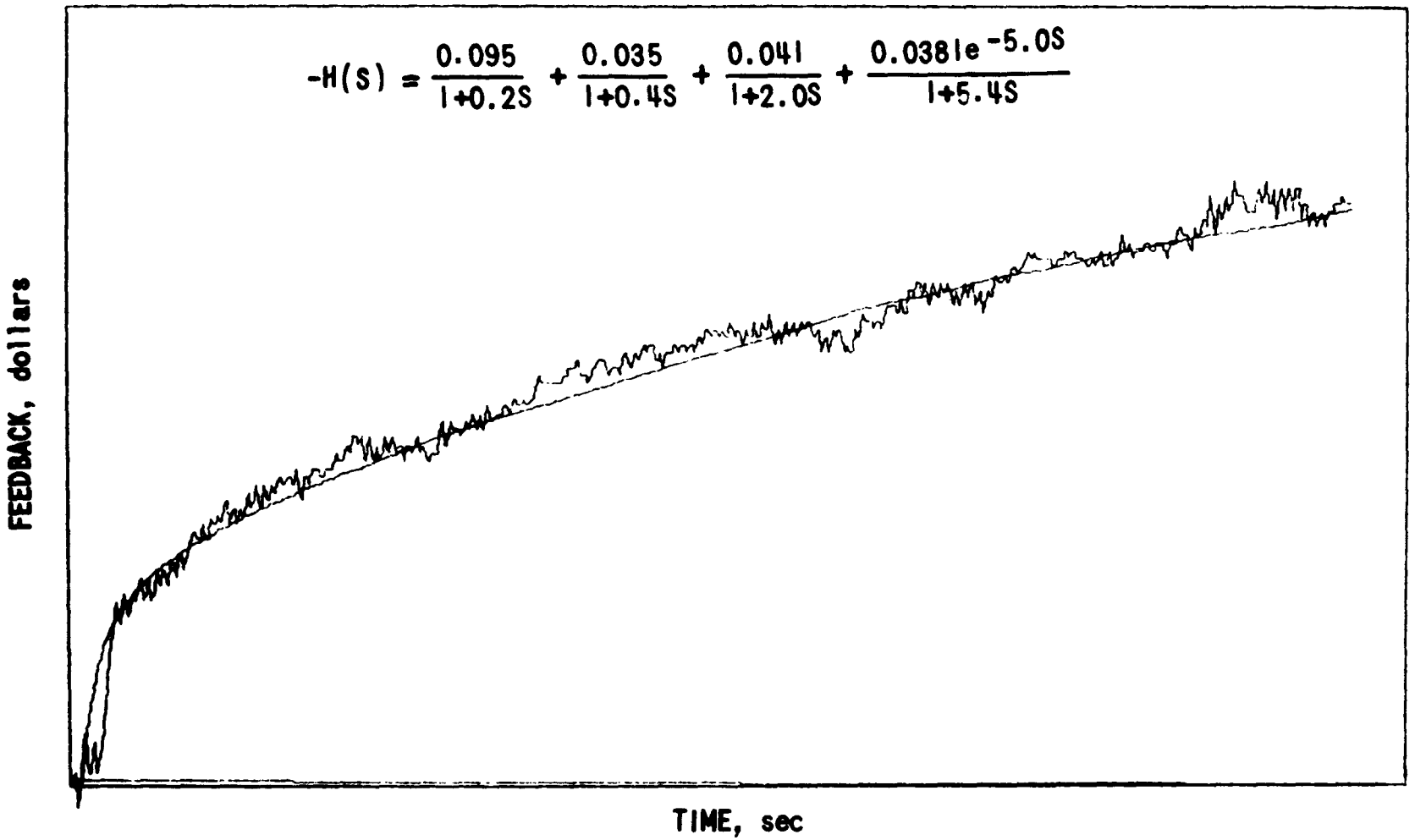

Fig. 6. Comparison of Measured 62.5-MWt Feedback with Feedback-reactivity Curve Calculated from 56-MWt Data; Start of Run 46A

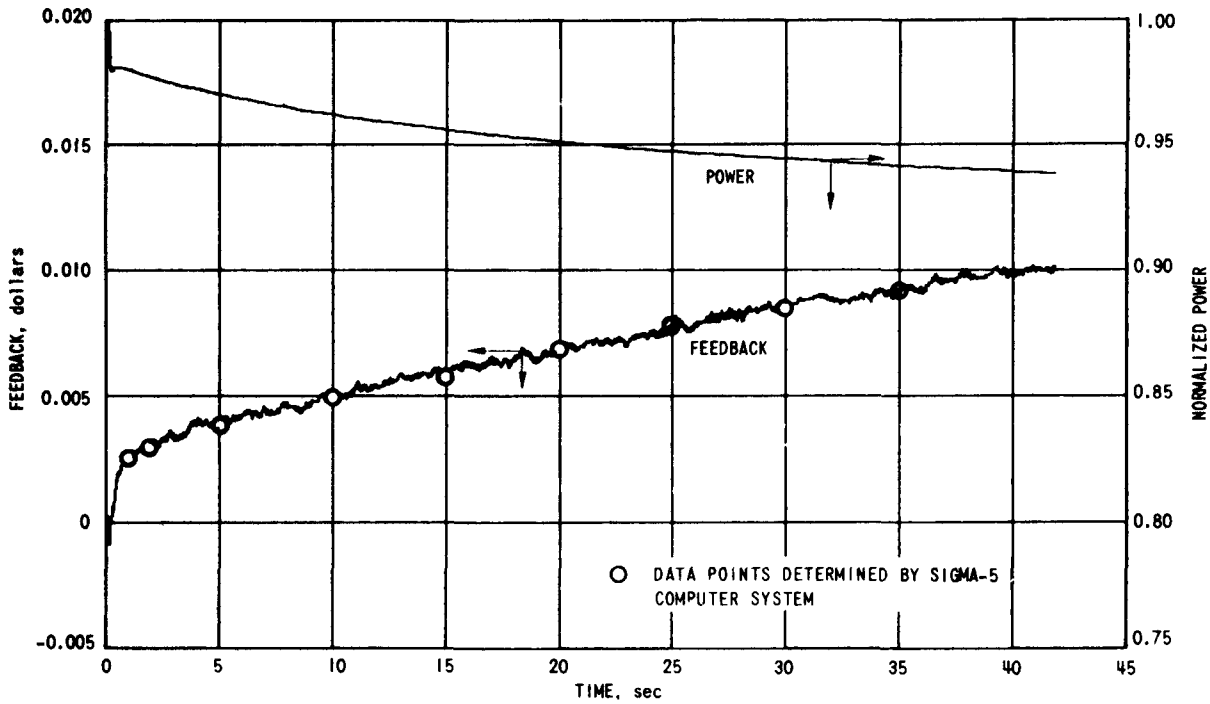

Fig. 7. Comparison of Feedback Function as Measured by Conventional and Sigma-5 Methods

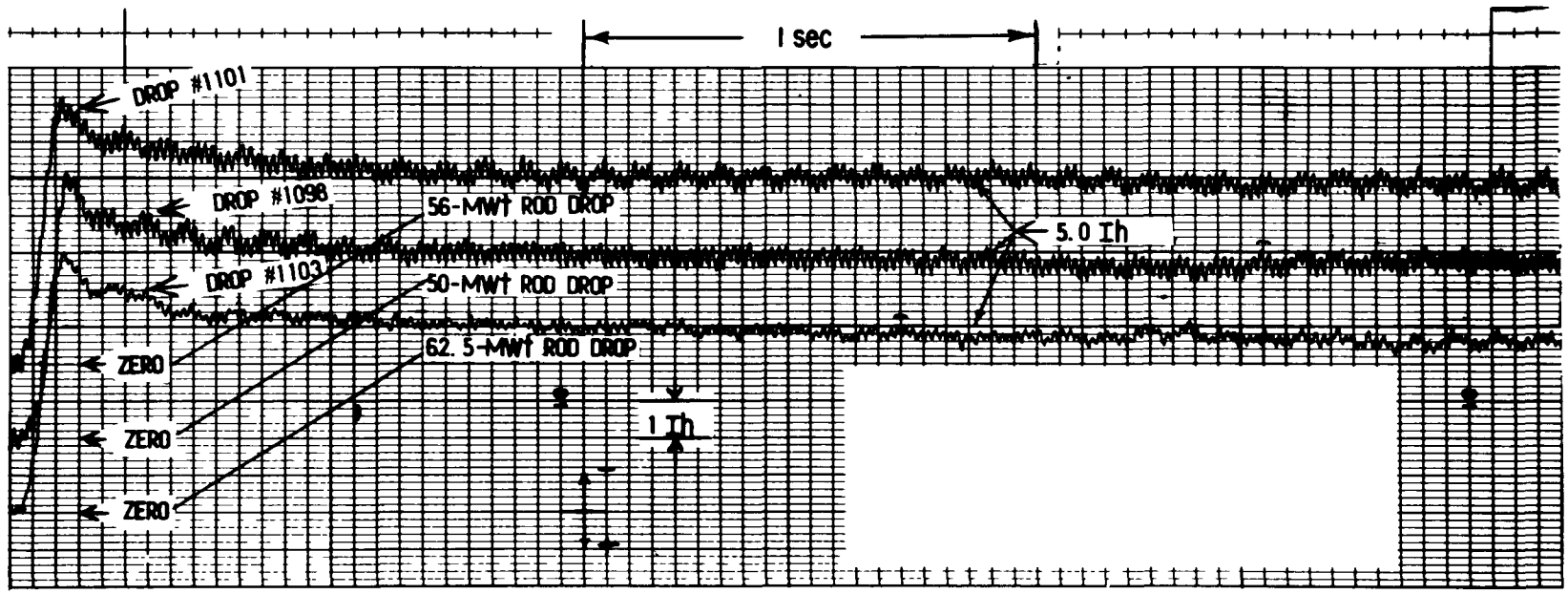

Fig. 8. Recordings made with On-line Reactivity Meter for Rod Drops at 50, 56, and 62.5 MWt in Run 46A

few tenths of a second after the drop. The feedback recovery had essentially the same time dependence as that established with the inverse-kinetics program. This fact suggests that the output of the reactivity meter may be used for rapid assessment of the operative feedback.

6. Subassembly-outlet Temperatures

Subassembly-outlet temperatures increased linearly with power during the power increase. Small deviations from expected values were noted, but these were of the same order as those usually noted.

7. Instrument Probe

During run 46A, the temperature distribution of coolant in the reactor outlet plenum was measured at a radius corresponding to a row-14 blanket position. Average temperatures recorded (beginning with the lowest thermocouple) were 882, 878, 871, 910, 925, 902, and 896°F. During run 38A in September 1969, corresponding temperatures were 853, 854, 858, 878, 881, 880, and 880°F. The small differences are believed caused by a change in the flow pattern in the plenum, which was caused by differences in the core loadings. The relationship between the pressure in the upper plenum (as indicated by pressure-sensing equipment on the probe) and flow rate did not change.

8. Noise-signature Analysis

Noise patterns were established for the neutron level and the two primary-sodium pumps at each steady-state power step in the ascent to 62.5 MWt. Figure 8 shows that a considerable 10-Hz noise component (in the neutron level) existed, particularly at 50 and 56 MWt. Also apparent in the figure is the indication that the amplitude of the 10-Hz noise decreased after the power level was raised to 62.5 MWt. As run 46A progressed, the amplitude continued to decrease and reached a level approximately 10-fold lower at the end of the run. During the shutdown at the end of run 46A, noise measurements were taken at 56, 50, and 40 MWt and at 500 kW. For all these, the amplitude remained small.

Noise patterns for the two primary pumps at 50 MWt at the start-up of run 46A were essentially the same as those established from earlier 50-MWt operation. Although no earlier pump-noise data for 62.5 MWt exist, the patterns established at 62.5 MWt during run 46A were consistent with data taken at 50 MWt.

The potential of using noise analysis for monitoring performance of the primary pumps was illustrated on September 29. On that date, the power demand for pump No. 1 gradually increased by 5 kW, but no change in primary flow rate was indicated. Shortly thereafter, the audible noise from pump No. 1 was louder than usual. Noise recordings were taken and showed a change in the normal noise pattern. Over a period of about an hour, the noise pattern reverted to its usual form. Concurrently, audible noise and power demand returned to normal.

Figures 9-13 show plots of the noise recordings (in the plots "G^{rms}" is the abbreviation for "gravity, root mean square"). Figure 9 shows plots taken with the MB accelerometer on primary pump No. 1 at 1500, from 0 to 20 kHz. During the time ($\sim$30 min) that the spectrum analyzer was being set up to record the data presented in Fig. 9, the pump noise was being observed on an oscilloscope; the noise appeared to decrease significantly from 1430 to 1500. Figure 10 shows data taken from 1515 to 1615 over the 0-100-Hz range; the noise appears to progressively decrease. Figure 11 presents data similar to that of Fig. 9 but taken at 1615, when the noise level had decreased. Figure 12 gives similar data taken at 2210, and shows no significant difference from that of Fig. 11. For comparison, Fig. 13 shows the noise data during the initial rise to power for run 46A. A more detailed coverage of the noise analyses is given in Ref. 7.

V. PLANT OPERATION

Surveillance of plant systems and components with the reactor operating at 62.5 MWt in run 46A verified satisfactory performance as anticipated. The operating parameters in Table V are essentially the same as during initial 62.5-MWt operation in run 38A. The differences in heat balances

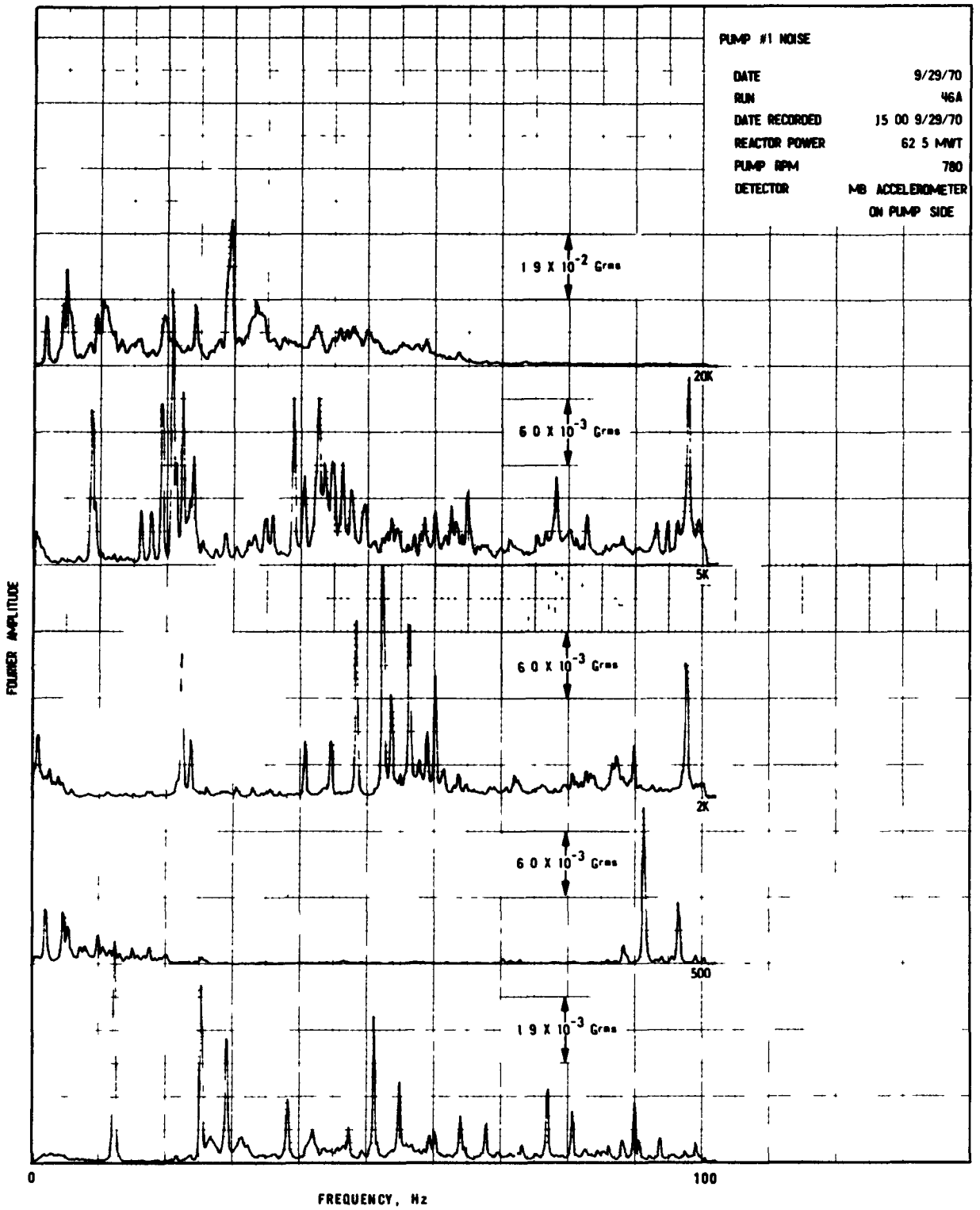

Fig. 9. Noise Recording for Pump No. 1 (0 to 20 kHz) at 1500, 9/29/70

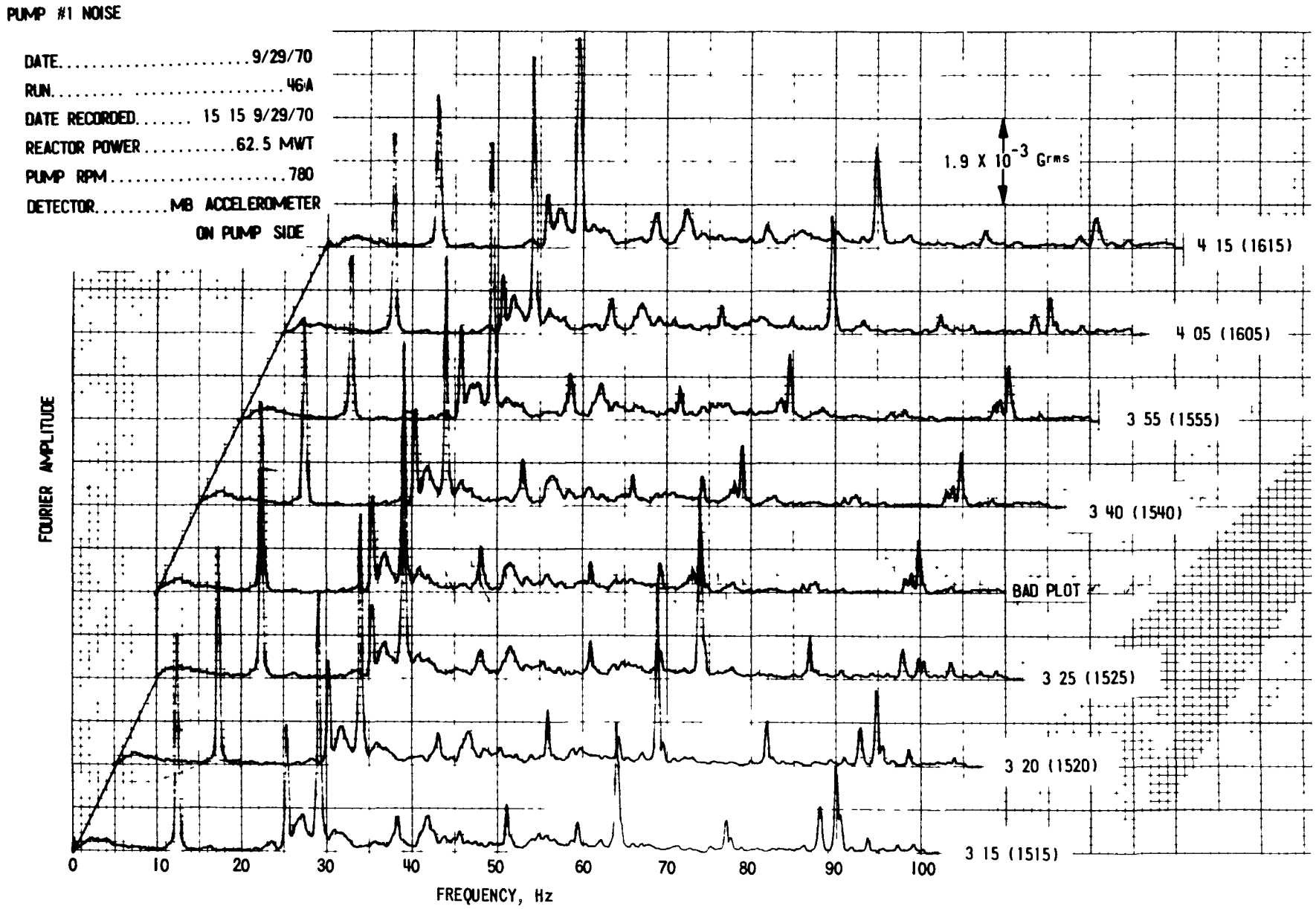

Fig. 10. Noise Recording for Pump No. 1 (0 to 100 Hz) 1515 to 1615, 9/29/70

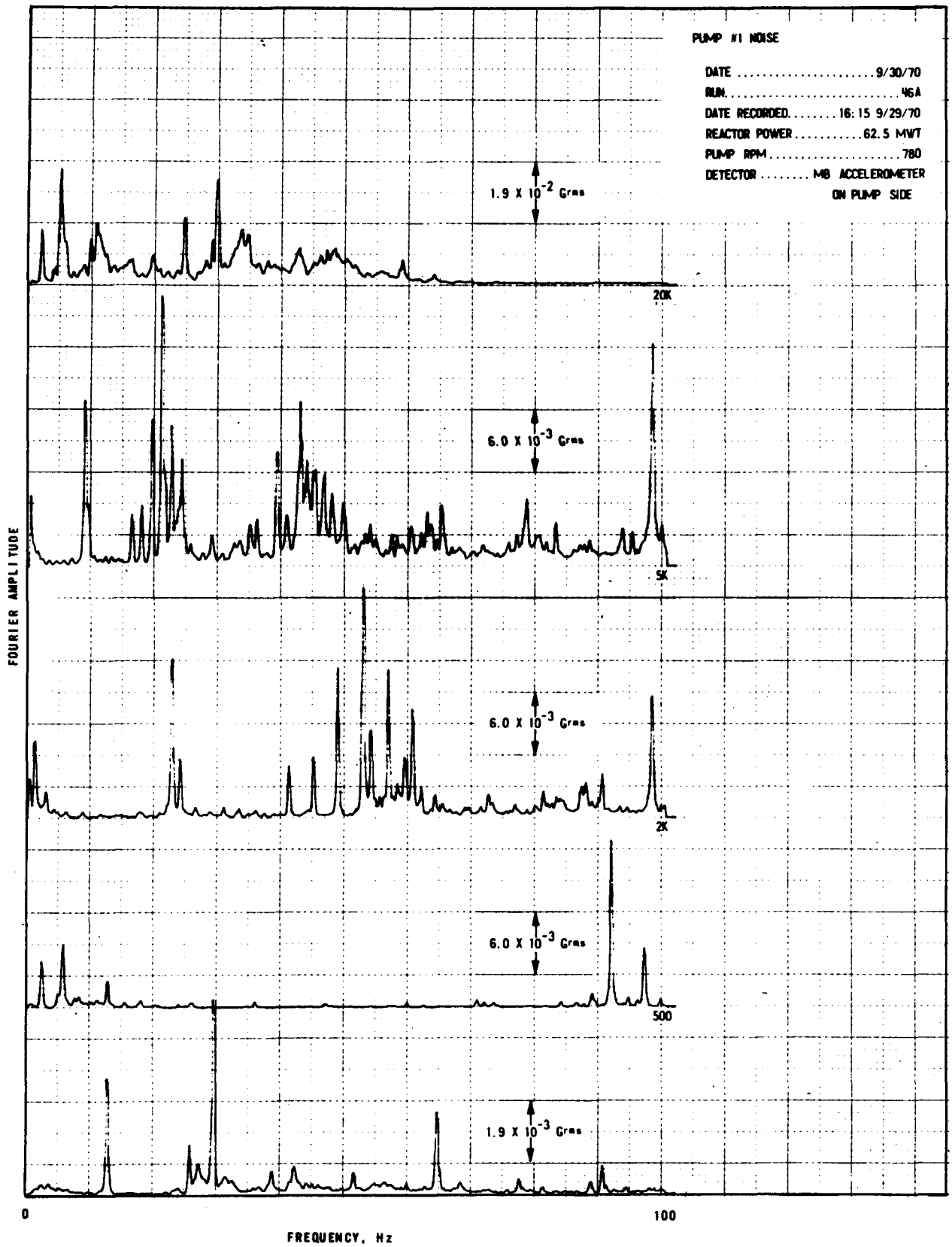

Fig. 11. Noise Recording for Pump No. 1 (0 to 20 kHz) at 1615, 9/29/70

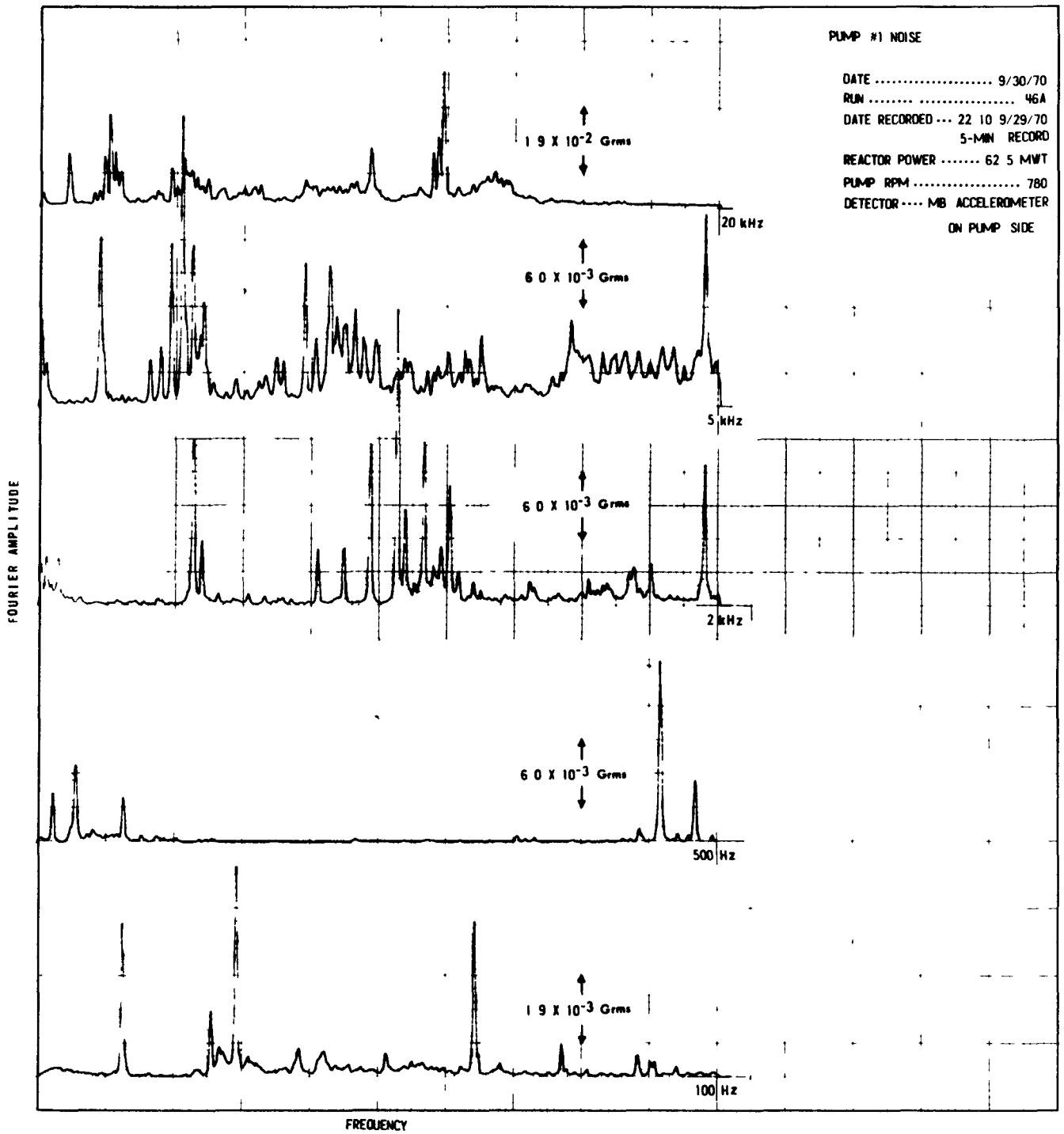

Fig. 12. Noise Recording for Pump No. 1 (0 to 20 kHz) at 2210, 9/29/70

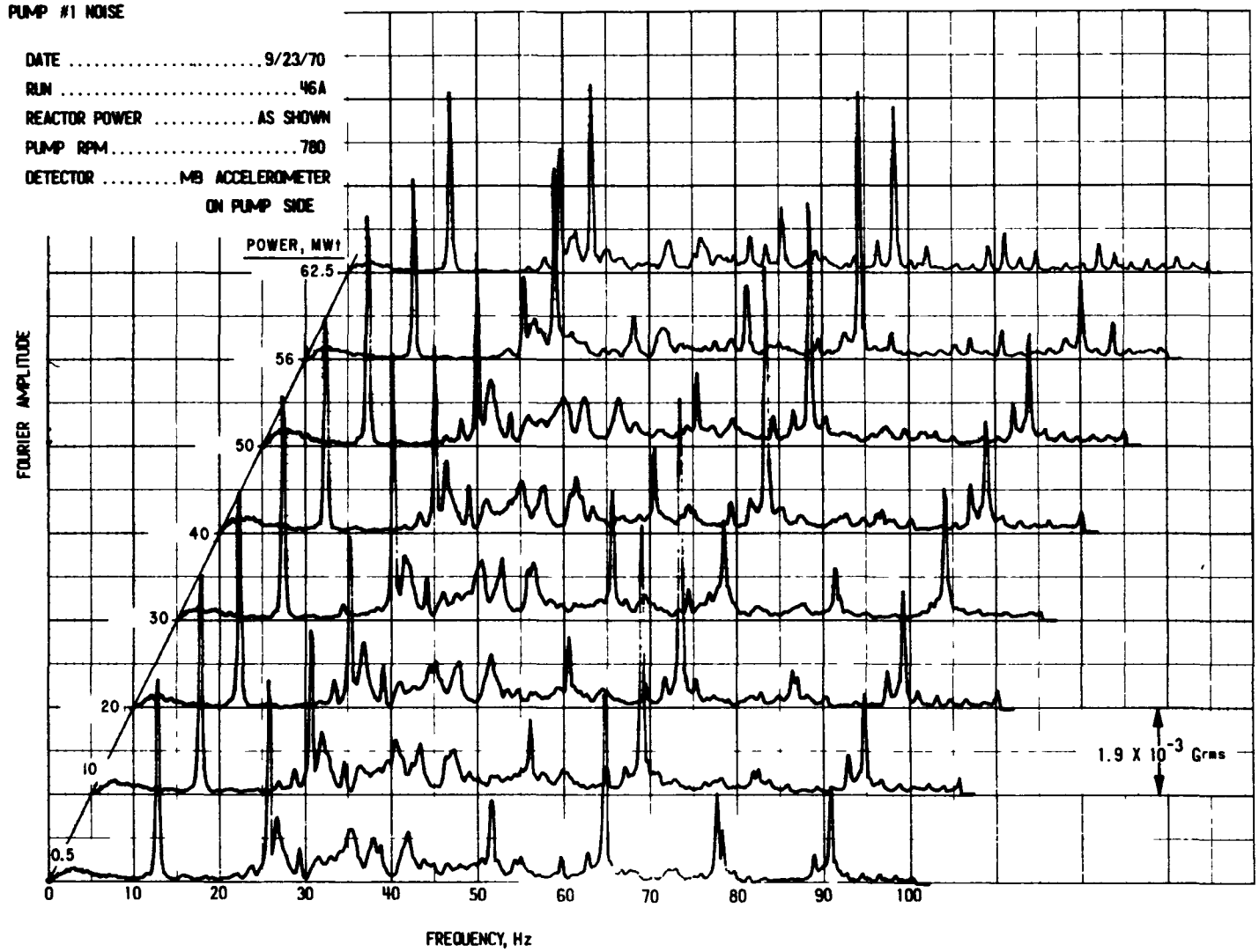

Fig. 13. Noise Recording for Pump No. 1 (0 to 100 Hz) as a Function of Power, during Initial Rise to 62.5 MWt, Run 46A, 9/23/70

TABLE V. Heat Balances and Component Parameters for Runs 38A and 46A

Parameter	56 MWt			62.5 MWt		
		Measured			Measured	
	Predicted[a]	Run 38A[b]	Run 46A	Predicted[a]	Run 38A[b]	Run 46A
Primary-system Power, MWt	56	56.5	55.8	62.5	62.3	62.3
Secondary-system Power, MWt	55.9	54.1	52.8	62.4	61.3	59.9
Steam-system Power, MWt	55.4	53.6	53.5	61.9	60.8	59.0
Intermediate Heat Exchanger						
Primary-sodium Flow Rate, 1000 lb/hr	3,820	3,860	3,810	3,820	3,810	3,810
Primary-sodium Inlet Temp, °F	864	864	864	883	883	883
Primary-sodium Outlet Temp, °F	700	700	700	700	700	700
Secondary-sodium Flow Rate, 1000 lb/hr	2,240	2,230	2,200	2,380	2,360	2,360
Secondary-sodium Inlet Temp, °F	584	588	588	585	586	588
Secondary-sodium Outlet Temp, °F	862	858	857	879	872	873
Steam Generator-Evaporators						
Secondary-sodium Inlet Temp, °F	791	788	785	803	800	802
Secondary-sodium Outlet Temp, °F	580	582	588	582	581	586
Feedwater Flow Rate, 1000 lb/hr	245	244	240	270	265	260
Feedwater Inlet Temp--Steam Drum, °F	549	559	550	549	560	550
Steam Outlet Temp, °F	579	580	583	579	580	582
Steam Generator--Superheaters						
Secondary-sodium Inlet Temp, °F	858	857	850	875	870	865
Secondary-sodium Outlet Temp, °F	791	788	785	803	800	802
Steam Flow Rate, 1000 lb/hr	225	224	220	250	250	241
Steam Inlet Temp, °F	578	580[c]	583	578	580	582
Steam Outlet Temp, °F	811	807	808	820	819	817
Turbine Generator						
Steam Flow Rate, 1000 lb/hr	146	148[d]	142	162	170	166
Steam Temperature, °F	811	807	808	820	819	817
Electrical Power, MWe	16.8	16.5	16.3	18.7	18.5	18.2

[a] From Ref. 1.

[b] From Ref. 2.

[c] Value previously reported in Ref. 2 as 559° due to typographical error.

[d] Value previously reported in Ref. 2 as 142,000 due to typographical error.

as measured in the primary and secondary sodium and the steam systems were greater during run 46A than during 38A; the discrepancy is again believed to be due to inaccuracy in temperature measurements.

A. Sodium Temperatures

The increase in power from 50 MWt to 62.5 MWt caused additional temperature stratification in the primary-system bulk sodium. This was expected, however, because earlier observations had indicated that stratification increases in accordance with reactor power. The effects of stratification in run 46A were like those of run 38A. Again, temperatures near the surface increased with power and those at the bottom decreased. Other studies, unrelated to run 46A, have suggested that bulk sodium mixing does take place in the central region of the tank but is not significant at the upper and lowermost sections. To a large extent the increased temperature at the upper level of bulk sodium and the slight decrease at the lower level may be attributed to natural convection. The rate of temperature rise in the upper-level sodium increases as reactor power is increased. The maximum difference in bulk sodium temperature at 50 MWt was 31°F. A thermocouple near the primary-secondary heat exchanger and reactor outlet piping registered a maximum temperature of 761°F at 62.5 MWt. Readings from this instrument fluctuated slowly over a range of 20-25°F, indicating that natural convection does occur in this section of the primary tank.

B. Steam System

A dynamic test of the steam-bypass system, condenser, and cooling tower was conducted during run 46A to determine:

1. Performance of power-plant systems when incoming-line circuit breakers were tripped with the reactor in normal operation at 62.5 MWt;
2. Performance of these systems when the turbine-generator output breaker was tripped under the same conditions; and
3. Performance of the main cooling tower at maximum load.

Operation at 62.5 MWt during run 38A had indicated unsatisfactory operation of the large steam-bypass valve. As a result, a new plug was

installed and the automatic controller replaced. Valve operation during run 46A was satisfactory.

When the incoming-line breakers were tripped, the large steam-bypass valve began opening in 2.3 sec, opened to 80% at 4.4 sec, and stabilized at 75% open. The steam pressure increased from 1264 to 1330 psig in about 2.0 sec, began decreasing at 2.5 sec, and then stabilized at 1290 psig at 8 sec.

By tripping of the generator output breaker, full plant steam load was placed on the steam-bypass system. The large steam-bypass valve began opening in 2.3 sec, opened to 90% at 4.5 sec, and stabilized at 80% open. The steam pressure increased from 1264 to 1332 psig in about 2.5 sec, began decreasing at 3.5 sec, and stabilized at 1296 psig at 10 sec.

To observe cooling-tower performance, the full steam load was bypassed directly to the condenser for about 2 hr after the breaker tests. The performance was satisfactory under existing atmospheric conditions.

Acoustical measurements were taken in each of the two superheaters during the increase of power to 62.5 MWt for run 46. The accelerometers used in these measurements were attached by magnets near the center of the superheaters on the shell surface.

The purpose of the monitoring was to obtain acoustic noise recordings of the noise generated in the superheaters during the increase in power. A primary objective was to attempt to obtain a flow-related characteristic noise spectrum, which could be used for reference in the analysis of future data that might be taken. The results are shown in Figs. 14 and 15, for the east and west superheaters, respectively. The data indicate a characteristic noise spectrum related to flow through the superheaters at higher flow rates. This spectrum begins to appear when flow through the superheater is about 1750 gpm (the flow rate for 30 MWt) and grows in amplitude as flow rate increases for higher-power operation. The frequency range of this noise is about 1-2 kHz. Figures 14 and 15 show that the same general spectrum existed on both superheaters.

The spectrum was examined up to 4 kHz at zero power and at varying power levels to 62.5 MWt. Above about 2 kHz no characteristic noise was detected. Below about 1 kHz no noise that could be correlated with flow through the superheaters was detected. The 60-Hz noise level in the

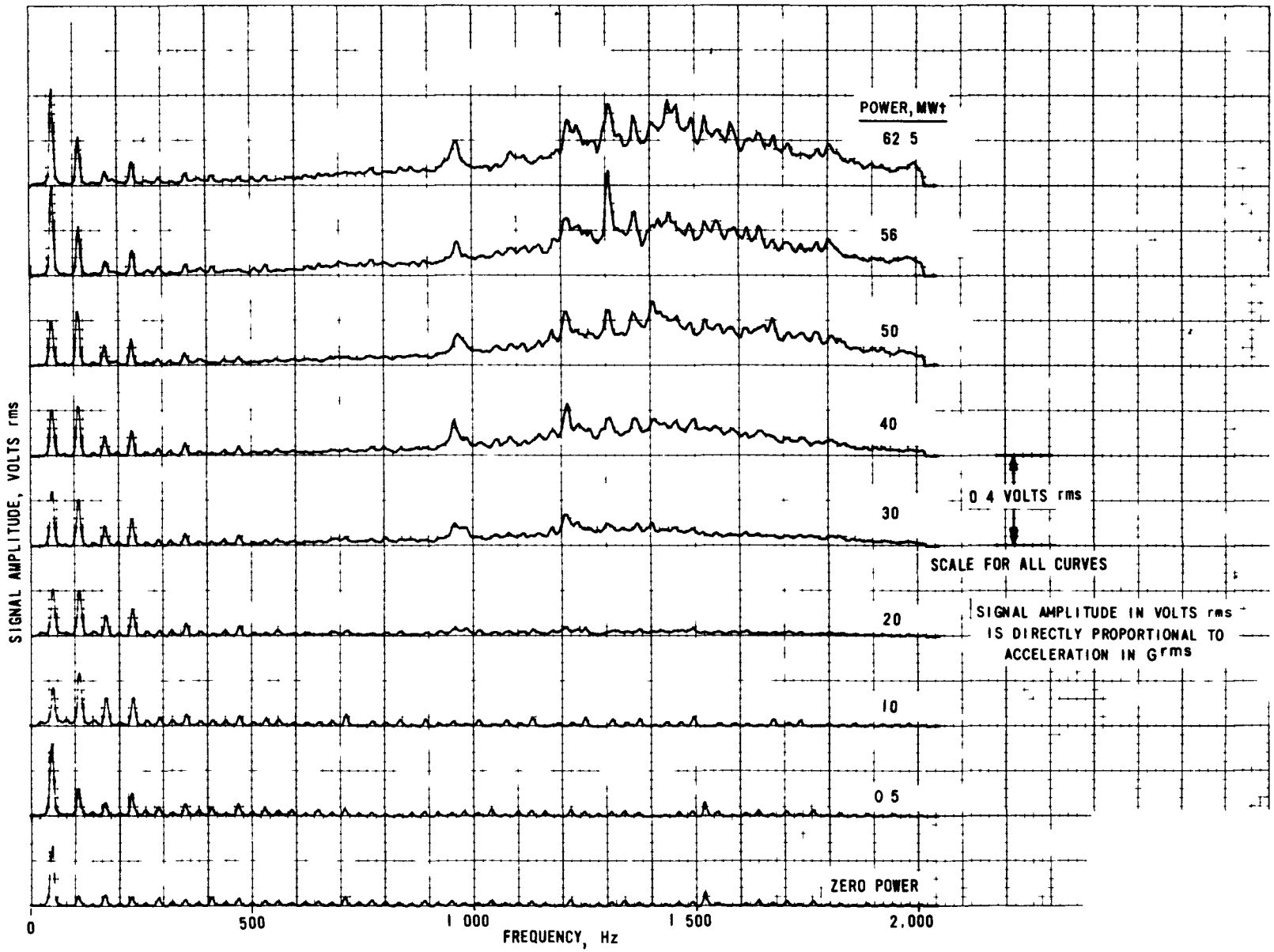

Fig. 14. Noise Spectrum as a Function of Power for East Superheater

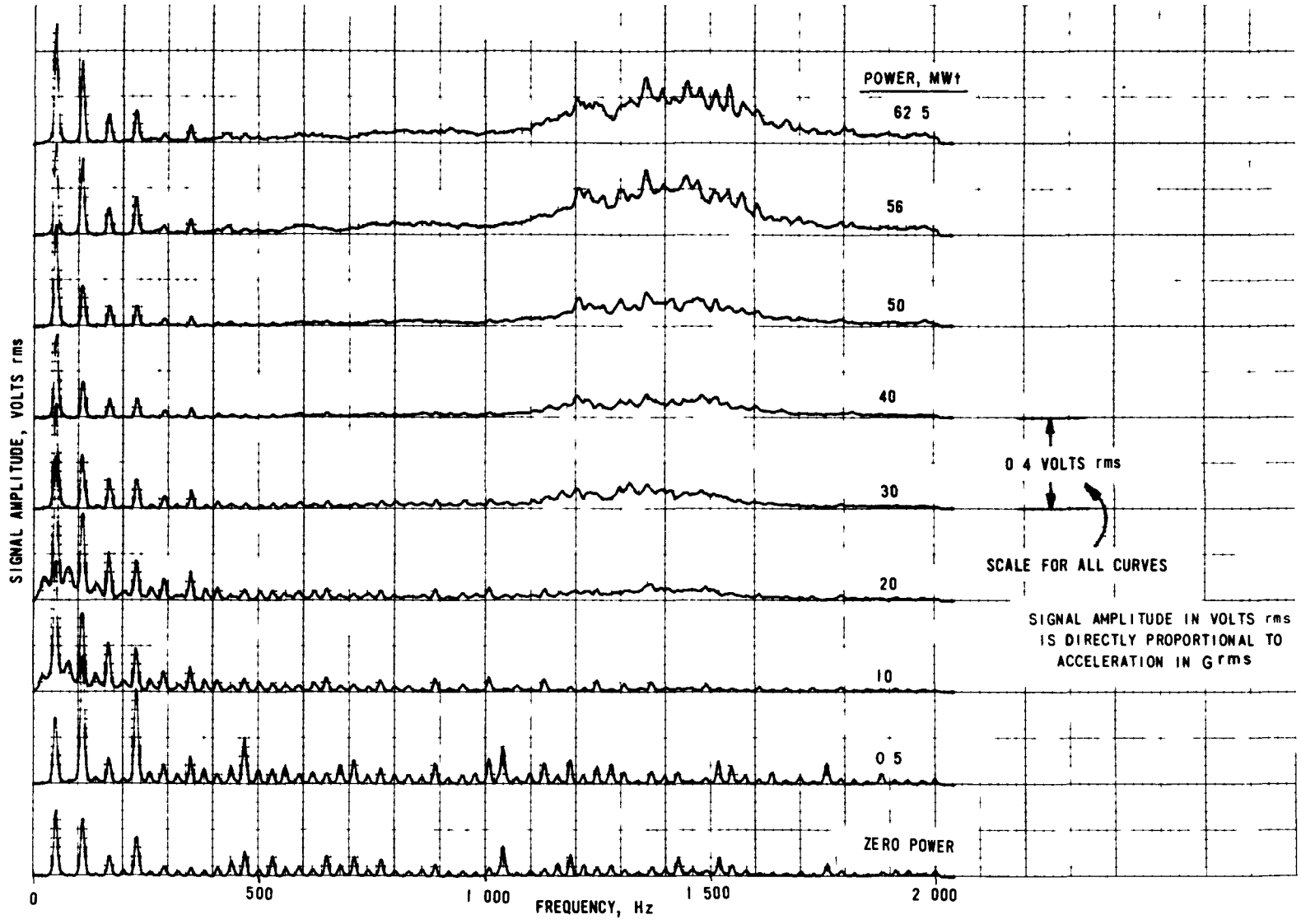

Fig. 15. Noise Spectrum as a Function of Power for West Superheater

sodium-boiler building limits low-frequency analysis. High levels of 60-Hz noise (and 60-Hz harmonics) were detected in the measuring system. However, the amplitude of these signals did not seem to be affected by changes in flow through the superheaters. In preparing the curves of Figs. 14 and 15 from the taped data, a high-pass filter was used to attenuate the 60-Hz noise and harmonics.

The following equipment was used in obtaining the data: Gulton Model AQB4971 accelerometers, an MB Electronics Model 9402216 line driver and Model N-400 charge amplifier, a Sangamo Model 3562 tape recorder, and a Spectral Dynamics Model SD301 spectrum analyzer. Comparing data collected during the run-46A startup with that collected during run 38A was originally planned. However, no correlation exists. One reason for this difference is that the band widths of frequency response of the two measuring systems used differed. Earlier, the system-frequency response was limited to about 500 Hz, whereas during run 46A the response was up to 4 kHz.

As expected, either of the installed feedwater pumps was capable of carrying the total feedwater flow at 62.5-MWt operation. Performance of the turbine-driven pump is slightly better than that during run 38A. Repair of the check valve increased the apparent capacity of the turbine-driven pump enough to make it unnecessary to shut off the pump recirculation flow at full power.

The performance of the motor-driven pump remains the same as it was during run 38A. The pump is running wide open at 62.5 MWt. As previously discussed in Ref. 3, a recirculation-control valve will be installed on this pump to increase its capacity about 13%.

The overload condition on the 480-V switchgear bus that would exist in the event of operation of a single power transformer has been eliminated by addition of cooling fans on each of the two 2000-kVA transformers. The fan-cooled capacity is 2300 kVA each. Measured 480-V load at 62.5 MWt operation is 2300 kVA.

The 480-V system load will be reduced further by the transfer of the Laboratory and Office Building 752 feeder from the main switchgear to the APPR standby substation. This work is in process.

A new 480-V substation has been purchased and the installation drawings are being prepared. This substation will remove all non-reactor-associated loads from the power-reactor plant switchgear.

The slight overload on the 2.4-kV switchgear can be handled within the 10% continuous-overload capability of the transformer. Cooling fans to further increase the capability of these units will be ordered.

VI. OPERATING PROCEDURES AT 62.5 MWt

Before run 46A, the control-room copies of the Operating Manual had, with two exceptions, been revised to cover reactor and plant operation at 62.5 MWt. The two exceptions were the list of operating set-points (Appendix G of the Manual) and the interlock check sheets (in Section II.A), which were written for a maximum power of 50 MWt. These sections were not revised after run 38A because it was not planned to return to 62.5 MWt operation for about another year. The same was true of the operating data sheets. Therefore, in preparation for run 46A, a special operating procedure, No. SOP 102-70, was issued. This SOP contained the necessary revisions to the check sheets, data sheets, and set points to reflect the expected parameters based upon the previous operating experience at 62.5 MWt. Only minor changes were required to reflect the actual values obtained.

VII. CONCLUSION

Operation of EBR-II at 62.5 MWt during run 46A was as expected. Continual operation at this power level is recommended.

REFERENCES

1. R. A. Cushman, Coordinator, Proposal for EBR-II Operation at 62.5 MWt, ANL/EBR-012 (August 1969).
2. R. A. Cushman, Coordinator, Operation of EBR-II at 62.5 MWt, An Evaluation of Plant and Reactor Data from Run 38A, ANL/EBR-013 (December 1969).

3. Prospectus: Routine Operation of EBR-II at 62.5 MWt, ANL/EBR-019 (to be published).

4. H. A. Larson and I. A. Engen, Collection and Evaluation of Kinetics Data from Run 46A, ANL/EBR-028 (to be published).

5. R. W. Hyndman and R. B. Nicholson, The EBR-II Feedback Function, ANL-7478 (July 1968).

6. R. W. Hyndman, R. O. Haroldsen, and J. R. Karvinen, EBR-II Digital Data Acquisition System Study, ANL/EBR-001 (May 1969).

7. C. C. Price and J. R. Karvinen, EBR-II Noise-signature Analysis During the First Half of Fiscal Year 1971, ANL/EBR-036 (to be published).